ACS Photonics

pubs.acs.org/journal/apchd5

Article

Optical Characterization of Silicon Nitride Metagrating-Based Lightsails for Self-Stabilization

Ramon Gao, Michael D. Kelzenberg, Yonghwi Kim, Ognjen Ilic, and Harry A. Atwater*

Cite This: https://doi.org/10.1021/acsphotonics.1c02022

Read Online

ACCESS | Metrics & More | Article Recommendations | Supporting Information

ABSTRACT: We report ultrathin photonic metagratings where anisotropic scattering is designed to achieve self-stabilizing dynamics in a collimated beam of laser light. Stability necessitates a delicate balance between all scattered orders of light, which we demonstrate in a monolithic material platform suited for efficient propulsion in space. Our suspended structures are fabricated in silicon nitride membranes, which is a promising lightsail material candidate due to its wafer-level scalability and favorable mechanical and optical properties. Lightsail prototype designs are optically characterized by angle-resolved photocurrent measurements of the intensities and angles of the asymmetric ±1 diffraction orders. We infer the optically induced forces and torques from refracted and reflected light measurements and show that these are restoring along one axis by providing them as input functions to numerical simulations of lightsail dynamics. Our experimental results represent a first step toward full dynamical verification of realistic lightsail designs and pave the way for realization of stable beam-riding lightsails composed of ultrathin dielectric membranes.

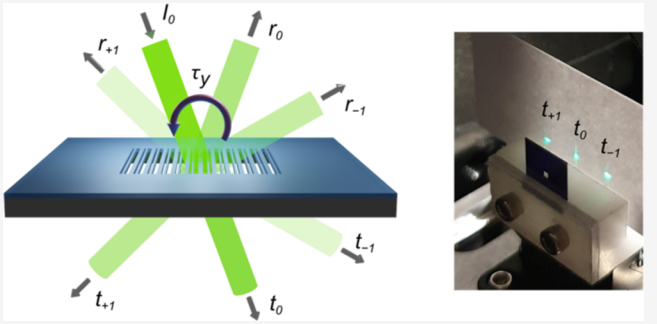

KEYWORDS: *Breakthrough Starshot, optical manipulation, optomechanics, metasurface, angle-resolved scattering, passive stabilization*

INTRODUCTION

Development of a spacecraft suitable for exploring the vast unknown beyond our own solar system within a human lifetime is currently defined by the travel time, which is limited by the ejection velocity of fuel from a rocket, as well as the amount of fuel one can carry onboard, as illustrated by Tsiolkovsky's rocket equation. Laser-propelled lightsails made of ultrathin, ultralight, and meter-sized reflective and non-absorbing membranes accelerated to significant fractions of the speed of light, as envisioned by goals of the Breakthrough Starshot Initiative have been highlighted as a viable means to overcome these limitations.[1,2] However, for such missions to be successful, one has to be able to control the lightsail trajectory over the entire propulsion impulse and ultimately over the entire travel distance. Passive stabilization of lightsail dynamics via nanophotonic structures patterned onto a lightsail depicts a promising step toward attitude control.[1,3] Numerous designs for self-stabilizing flat lightsails have now been studied theoretically, including diffractive structures such as bigratings[4] and axicons,[5] metagratings,[3] nonlinear photonic crystals,[6] metasurfaces,[7−12] and damped mechanical internal degrees of freedom.[13] First experimental investigations into stable beam-riding behavior have focused on materials such as nematic liquid crystals[14] and photopolymers on sapphire.[15] However, for ultrathin lightsails to survive the extreme laser power densities (>1 MW/cm^2) for Starshot lightsail propulsion conditions, materials with ultralow absorption are required such as low-loss dielectrics and semiconductors, which can avoid substantial thermal heating,[1,16,17] in addition to thermal management strategies on enhancing the emissivity in the thermal wavelength regime.[16,18,19]

In this paper, we design, fabricate, and characterize a dielectric optical metagrating for passive stabilization based on mirror-symmetrically arranged one-dimensional metagratings (Figure 1a). While self-stabilizing optical designs implemented on the silicon-on-insulator platform have hitherto been studied,[3,7−9,12] we identify silicon nitride as a leading material candidate due to its potential for ultralow absorptivity[20,21] on the order of 10^{-5} to 10^{-6}, sufficiently high index contrast, robust mechanical properties, and wafer scalability.[22] With its large band gap pushing the threshold for thermal runaway due to two-photon absorption as reported for silicon to higher temperatures[23] and allowing for laboratory-scale experiments in the visible wavelength regime, its high intrinsic stress has been instrumental in realizations of high-reflectivity and high-Q membrane-based optomechanical resonators.[24−28] Moreover, suspended one-dimensional silicon nitride gratings have been

Received: December 31, 2021

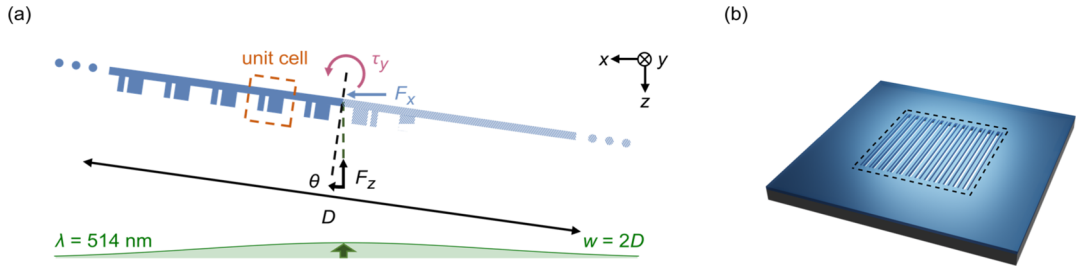

Figure 1. (a) Schematic of a passively stabilized rigid lightsail based on the mirror-symmetric arrangement of optical metagratings about the center of mass. Optically induced optical forces and torque due to a weakly focused Gaussian beam are responsible for propulsion (F_z) and self-restoring behavior (F_x, τ_y). (b) Patterned silicon nitride membranes (dashed lines indicate active area) as an experimental platform to assess the optical and mechanical response of etched metagratings for passive stabilization along one axis.

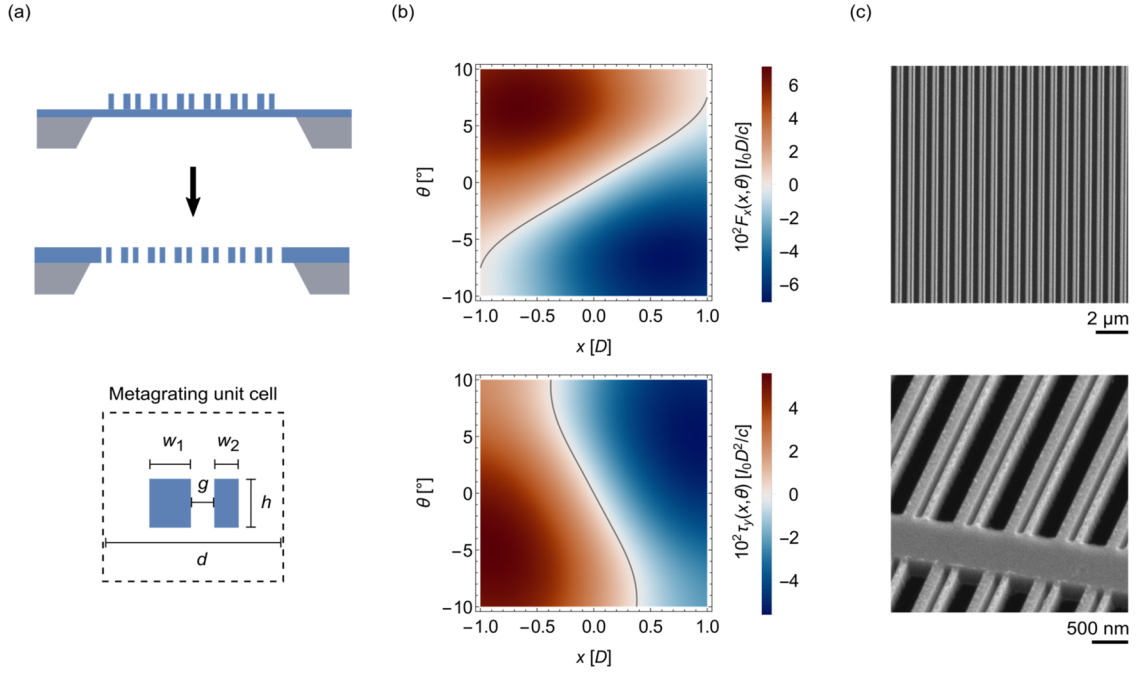

Figure 2. (a) Schematic of our choice to design and fabricate a self-stabilizing silicon nitride metagrating without a substrate, i.e., with only two dissimilar rectangular resonators. The asymmetric unit cell of the identified self-stabilizing metagrating is described by w_1 = 170 nm, w_2 = 100 nm, g = 95 nm, d = 720 nm, and h = 200 nm. (b) Simulated induced restoring lateral force (top) and in-plane torque (bottom) on mirror-symmetrically arranged metagratings plotted vs translation x and rotation θ, with contour lines depicting F_x = 0 and τ_y = 0. Self-stabilization is characterized by a negative slope along the horizontal (vertical) line at θ = 0° (x/D = 0) for F_x (τ_y) when going from negative to positive translation (rotation). (c) SEM images of fabricated 120 × 120 μm-sized metagrating prototypes, with 20 μm long gratings being mechanically supported by 1 μm wide anchor bars.

demonstrated for applications in sensing, optical filtering, and differentiation.[29−31] In fact, one-dimensional subwavelength gratings were shown to result in more efficient lightsail propulsion compared to previously reported optimal photonic geometries.[32] Consequently, our approach is rooted in combining the suspended silicon nitride membrane architecture with optical metagrating designs, the fabrication of which demonstrates natural scalability from microscopic to large-scale demonstrations of dynamical stability (Figure 1b). To characterize the optical response of our fabricated metagrating sample and deduce dynamical stability, we quantify the carefully designed relationship between all diffracted orders by rotating a photodetector around our device, with similar setups developed for angle-resolved scattering experiments.[33−36] By inferring the optically induced forces and torques from diffraction measurements, we introduce a silicon nitride photonic design as a candidate prototype for self-stabilizing lightsails for applications ranging from contactless far-field optical manipulation to spacecraft propulsion.[37−40]

RESULTS AND DISCUSSION

While previously reported optical designs for stable beam-riding featured resonators on a substrate, we found that removing the substrate by fully etching through silicon nitride films does not comprise our ability to identify metagrating designs for passive stabilization (Figure 2a). Such an approach helps in meeting the strict mass budget for ultralight lightsails, simplifies the fabrication process, and minimizes the chances of possibly obscuring phenomena such as coupling to guided modes and other loss channels. On the other hand, reduced structural stability and induced stress concentrations will need to be carefully evaluated. Choosing the h = 200 nm tall resonators to be of dissimilar widths will result in an anisotropic optical response with respect to the incidence

https://doi.org/10.1021/acsphotonics.1c02022
ACS Photonics XXXX, XXX, XXX−XXX

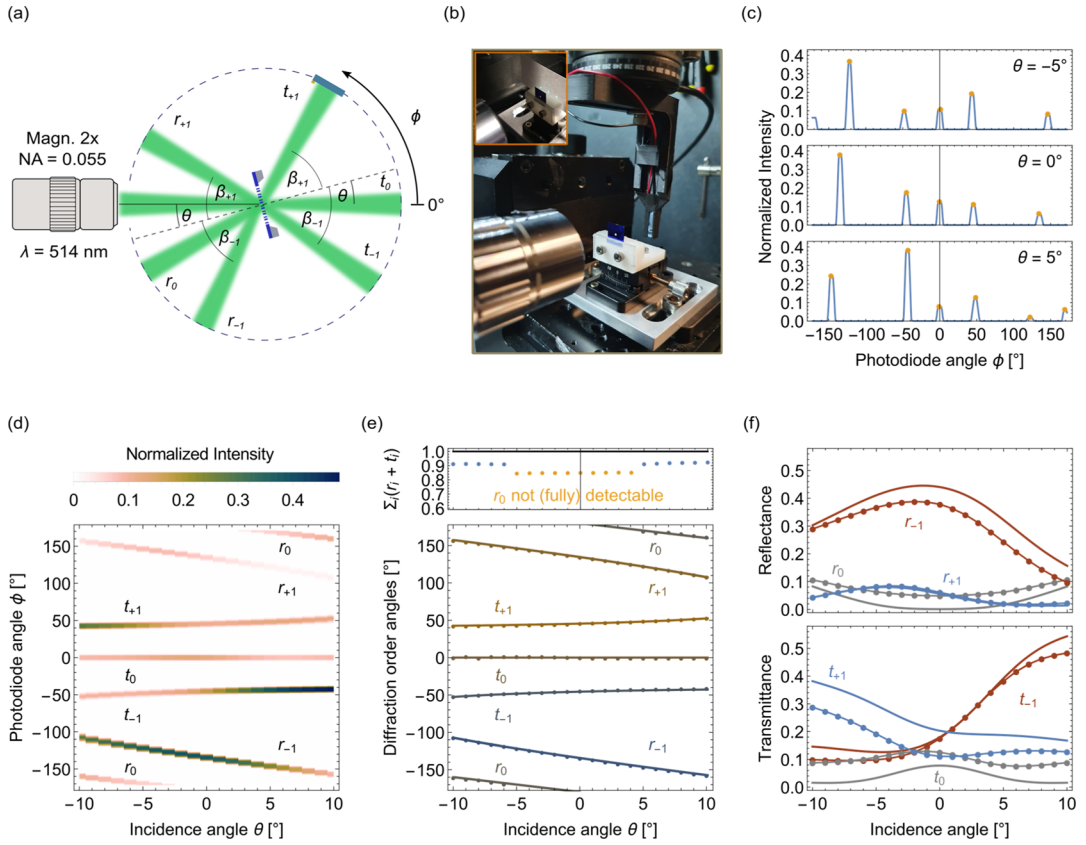

Figure 3. (a) Schematic of the angle-resolved photocurrent measurement setup for metagrating characterization. (b) Photo of the setup with objective, sample mounted on a translation-rotation stage, and movable photodiode. Inset shows the transmitted diffracted orders of the metagrating for incident light. (c) Refracted and reflected light measured with the photodiode for various incidence angles, showing anisotropic diffraction of light by the metagrating. (d) Visualization of the entire data set measured by the photodiode as a density plot with a color scale indicating the normalized intensities of all diffraction orders. (e) Sum of refracted and reflected light normalized intensities compared against baseline (black) with the specularly reflected order being not detectable for small incidence angles (top) and comparison of theoretically calculated diffraction order angles using the grating equation with measured angles (bottom). (f) Comparison of experimentally measured (dotted lines) reflectance (top) and transmittance (bottom) vs simulated (solid lines) reflectance (top) and transmittance (bottom) as a function of incidence angle.

angle if these structures are illuminated by a plane wave. For incident light at λ = 514 nm, a wavelength that is shorter than the targeted near-infrared laser wavelength for the Starshot mission but would allow for the first radiation pressure experiments of lightsail candidates in the visible region with relatively low absorption losses using an existing laser source in our laboratory, we limit our design search to designs supporting $m = \pm 1$ diffraction orders. By systematically varying the geometry of the metagrating unit cell, we arrived at the self-stabilizing metagrating design depicted in Figure 2a. With its geometry described by d = 720 nm, h = 200 nm, w_1 = 170 nm, w_2 = 100 nm, and g = 95 nm, its anisotropic diffraction of light gives rise to angle- and position-dependent restoring lateral force $F_x(x,\theta)$ and in-plane torque $\tau_y(x,\theta)$ per unit length in the y-direction shown in Figure 2b, where we have assumed a Gaussian beam profile described by $I(x) = I_0 \exp(-2x^2/w^2)$ with beam width $w = 2D$ and its electric field polarized along the grating direction. Both $F_x(x,\theta)$ and $\tau_y(x,\theta)$ are necessarily zero at the equilibrium position $x = 0$ for a nontilted lightsail. While a restoring lateral force must exhibit a negative slope versus displacement, the shape of the restoring in-plane torque should satisfy $\tau_y(\theta) \tan(\theta) < 0$ around $\theta = 0°$. We note that the gray isolines denoting where the lateral force or in-plane torque is zero are diagonal with respect to x and θ, whereas in an unpublished study on spinning lightsails, we have found metagrating designs, where the zero crossings of lateral forces are robust against rotations and are thus represented by vertical isolines. With further studies needed to be conducted, this observation may hint at different optimization objectives for self-stabilizing nonspinning and spinning lightsails.

One of our successfully fabricated samples is shown in Figure 2c, with the scanning electron microscopy (SEM) images confirming our designed geometry. Given a metagrating size of 120 × 120 μm and the etched-through geometry, we included 1 μm-wide anchor bars every 20 μm in the y-direction to mechanically reinforce the suspended subwavelength-sized resonators and prevent stiction between them.

Using our custom-built angle-resolved photocurrent measurement setup to optically characterize our metagrating samples (Figure 3a,b), we experimentally determined the refracted and reflected light intensities versus incidence angle in the range of −10 to 10° in steps of 0.5°. Snapshots of these angle-resolved measurements at three incidence angles are shown in Figure 3c, where we used a peak identification algorithm on the photocurrent data, followed by a Gaussian filter to extract the normalized intensities and directions of all scattered orders. We observe the anisotropy in the diffraction

https://doi.org/10.1021/acsphotonics.1c02022
ACS Photonics XXXX, XXX, XXX−XXX

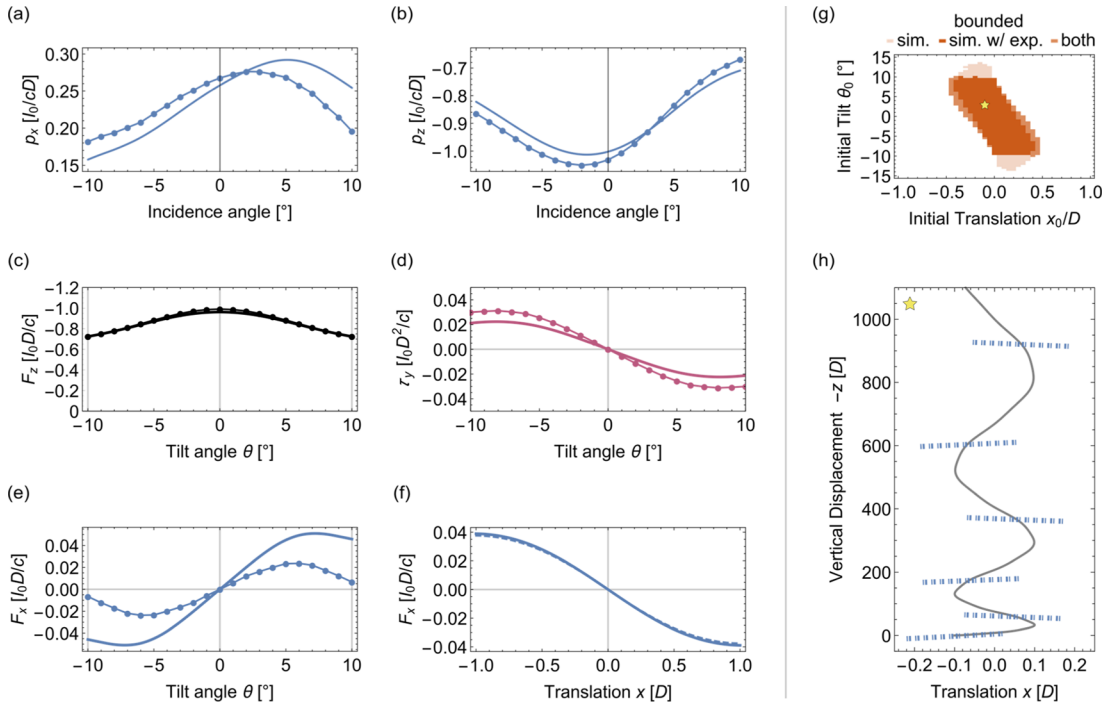

Figure 4. (a,b) Comparison of simulated (solid lines) and from measurements inferred (dotted lines) pressures, (c) angle-dependent lateral force, (d) translation-dependent lateral force, (e) angle-dependent vertical force, and (f) angle-dependent torque. $F_x(x)$ is inferred from measured scattering at $\theta = 0°$ and plotted as a dashed line to indicate that every data point can be derived solely from $p_x(\theta = 0°)$. (g) Initial conditions for bounded dynamics of lightsails patterned with the ideal theoretical metagrating design vs the actually fabricated metagrating. A trajectory is denoted as bounded if $|\theta(t)| \leq 15°$ and $|x(t)| \leq 1.5D$ for $t = 0 \ldots 1000t_0$, with $t_0 = (mc/I_0)^{1/2}$. (h) Example trajectory of a metagrating passively stabilized by optical forces and torque inferred from measured diffraction for an initial tilt of 3° and translation of $-0.1D$.

data due to the asymmetric metagrating design when comparing the angle-resolved intensities at $\theta = -5°$ to those at $\theta = 5°$. Anisotropic diffraction becomes even more apparent when visualizing the entire data set as measured by the photodiode as a density plot in Figure 3d. Despite the symmetry in angles ϕ of the ± 1 diffraction orders versus incidence angle, their normalized intensities differ from each other at $\pm\theta$, with differences being more pronounced for the transmitted orders. While we are able to measure all diffracted orders at larger incidence angles, for small θ—corresponding to near-normal light incidence conditions—specularly reflected light is directed back into the objective and thus not measurable in our setup as moving the photodiode into these positions would block the incident beam, thus resulting in five instead of six peaks. This experimental limitation is the reason for the reduced sum of refracted and reflected light intensities in Figure 3d for incidence angles between −5 and +4°. We note that the asymmetry stems from the photodiode being mounted slightly off-centered onto the holder. To overcome the limitation in measurement of the specularly reflected order for small θ, we fitted these data points measured at larger θ to a quadratic function, given that the simulated specularly reflected order follows a parabola-like shape, and appended the fitted values at small θ to the incomplete set of recorded specularly reflected order intensities (Figure S2). Nevertheless, we observe that for larger incidence angles, our experimentally measured sum of diffraction intensities does not fall below 85% of the baseline, that is, incident light on the photodiode with no sample in between. Reasons for the normalized refracted and reflected light intensities not summing up to unity include out-of-plane scattering of light due to the anchor bars and surface roughness and finite absorption in our low-stress silicon nitride structures, which we attribute mainly to the low-stress membrane synthesis process and possibly also to residual damage in nanofabrication.

Comparison of the experimentally determined diffraction angles with the solutions to the grating equation $m\lambda/d = \sin(\beta_m) - \sin(\theta)$ with $m = 0, \pm 1$ for the range of studied incidence angles, reveals excellent agreement (within ±1°), which for the selected wavelength of incident light confirms the fabricated period of our metagrating sample (Figure 3e). The inability to detect specularly reflected light for small θ due to obstruction of the incident light path by the finite-sized photodiode is reflected in the y-axis of Figure 3e, being limited between −170 and 169°. In Figure 3f, we compare the measured angle-dependent normalized intensities of diffracted light to simulated reflection and transmission coefficients r_m and t_m, respectively, and note that differences can be observed between the measured and calculated values. In general, the same functional form is observed for all r_m and t_m with angle. While a better agreement is found for r_{+1} and t_{-1}, all other coefficients exhibit greater discrepancies between measurement and calculations, as can be seen from the offsets in magnitude. A closer look at SEM images taken of our fabricated samples reveals minor differences between the fabricated dimensions and their target values of up to 5 nm, as well as partially roughened top and bottom surfaces and nonvertical sidewalls, all of which can result in altered diffraction behavior and additional isotropic light scattering. Moreover, we found that the mechanically supporting anchor bars contribute to diffraction of light in the vertical direction as opposed to diffraction in the horizontal plane by the metagratings. We found the anchor bars to be necessary, having fabricated

https://doi.org/10.1021/acsphotonics.1c02022
ACS Photonics XXXX, XXX, XXX−XXX

several metagrating designs with variable spacings between anchor bars. Specifically, we found that anchor bar designs whose periods were greater than 20 μm resulted in stiction of the thin grating resonators possibly occurring during the wet-chemistry-based resist stripping process. This type of structural distortion could be prevented by adjusting the metagrating design to ensure larger gaps between resonators or using silicon nitride with higher tensile stress and thus lower compliance. While our 17 mm-tall photodiode can capture the lowest diffraction orders, due to the 2-orders-of-magnitude difference in the anchor period to wavelength (20 μm to 514 nm), higher diffraction orders were not measurable. Other potential reasons could include the finite size of our metagratings, and the fact that the incident light was weakly focused instead of being a true plane wave.[41] For the latter, using an objective with a low numerical aperture (NA = 0.055) ensures a low divergence angle of a maximum 2° while focusing incident laser light to a small-enough spot size less than the metagrating size. By imaging the focused beam using a CMOS camera in the specimen plane, we determined its full width at half-maximum to be ∼60 μm (Figure S3). Consequently, substantially all of the laser intensity was incident on our metagrating, thus suggesting that edge effects from the outermost gratings could be neglected in our analysis.

The overall agreement in the anisotropic diffraction between experiment and simulation warrants calculation of the optically induced pressures in the inertial frame from the collection of refracted and reflected light using the photon momentum balance equation given by

$$\boldsymbol{p} = -\frac{I_0}{c}\left(e_z + \sum_{m=-1}^{+1}[t_m\sin(\beta_m - \theta) + r_m\sin(\beta_m - \theta)]e_x + [-t_m\cos(\beta_m - \theta) + r_m\cos(\beta_m - \theta)]e_z\right)$$

where I_0 and c correspond to the incident (peak) beam intensity and speed of light, respectively. As before, we observe overall qualitative agreement in the shape of curves for $\boldsymbol{p}$ barring small differences in the magnitude (Figure 4a,b). For a laser beam of Gaussian shape with width $w = 2D$ in agreement with the simulation results described earlier, the optically induced force $\boldsymbol{F}$ and torque τ_y as a function of translation and rotation can be derived. Calculation of these quantities assumes our characterized metagrating to represent the left half of the lightsail, with the geometry of its right half being determined by the imposed mirror symmetry. Juxtaposing optical forces and torques inferred from measured scattering with simulation results shows excellent agreement for F_z (Figure 4c) and reasonable similarity for τ_y (Figure 4d). On the other hand, the lateral force F_x shows both a reduced angular range of stability and slope at zero tilt (Figure 4e). The more notable difference in F_x between experiments and simulations could be explained by the above-mentioned discrepancies between measured and simulated reflection and transmission coefficients, which have a larger effect on F_x compared to F_z and τ_y, suggesting greater susceptibility of the angle-dependent lateral force to fabrication imperfections and design variations. For the lateral force, it is instructive to also plot F_x as a function of x, the lateral translation distance of the lightsail from the laser propulsion beam axis. The overall restoring behavior of the lateral force is confirmed by the negative slope of $F_x(x)$ through the equilibrium at $x = 0$ (Figure 4f). While future improvements in fabrication of suspended silicon nitride metagratings to remove unwanted scattering sources such as the anchor bars are possible to achieve better quantitative agreement between simulations and experiment, our silicon nitride metagrating prototype reported here already exhibits self-stabilizing behavior along one axis.

By numerically linearizing the partial derivatives of experimentally inferred $F_x(x,\theta)$ and $\tau_y(x,\theta)$ with respect to x and θ at the equilibrium (see the Supporting Information), we calculated the gradients and consequently relevant entries of the Jacobian matrix to be $f_{xx} = -0.063$, $f_{x\theta} = 0.329$, $f_{\theta x} = -0.958$, and $f_{\theta\theta} = -3.982$, resulting in eigenvalues $\Lambda_{1,3} = \pm 0.381i$ and $\Lambda_{2,4} = \pm 1.975i$, which suggests marginal stability for small perturbations in the vicinity of the beam center. To study the robustness of the stabilization mechanism in our device, we performed an error propagation analysis by assigning uncertainties to every measured quantity. Specifically, assuming a standard error (σ) of $\Delta r_0 = 0.05$ for the specularly reflected order, $\Delta r = \Delta t = 0.01$ for all other diffracted orders, $\Delta\beta = 1°$ for β_m, and $\Delta\theta = 0.1°$ for θ, corresponding variations of the gradients within the propagated error margins will still result in purely imaginary eigenvalues in the majority of studied cases, namely, ∼58%. This observation can be interpreted in two ways: while it suggests a certain degree of robustness of our device to fabrication imperfections and measurement uncertainties, it also highlights the necessity of ensuring a carefully designed relationship between all scattered orders to obtain self-stabilizing behavior.

Taking a step further, we provided estimates for the experimentally derived optical pressures as input functions to the equations of motion to simulate lightsail propulsion trajectories for a specified set of initial conditions, that is, finite lateral displacement x_0 and tilt θ_0 ranging from $-D$ to D and -15 to 15°, respectively (Figure 4g). All cases were numerically evolved for a total duration of $1000t_0$ with $t_0 = (mc/I_0)^{1/2}$, where m is the lightsail mass per unit length in the y-direction. We then analyzed all such trajectories and deemed these as being bounded if the absolute values of their maximum lateral and angular amplitudes did not exceed $1.5D$ and 15°, respectively.

By comparing the obtained map of initial conditions leading to stabilized trajectories for a lightsail patterned with our fabricated metagrating design with that based on the theoretical design, we observe that in general, the contiguous set of initial conditions that results in marginally stable trajectories is of similar size for the presented experimental structure compared to that for its theoretical counterpart. However, some more extreme initial conditions at $|\theta|$ larger than 10° only result in bounded dynamics for the purely simulated lightsail, whereas other extreme initial conditions with greater translations result in stabilized trajectories only for the simulated lightsail based on the characterized metagrating. This can be explained by the reduced angular range of stability and magnitude for experimentally derived F_x and the increased magnitude for experimentally inferred τ_y, as seen in Figure 4d,e, and in general, the limited range of measured incidence angles. Nevertheless, the results indicate that our experimental structures are consistent with self-stabilized trajectories for tilts of several degrees and translations of several tens of percent of the lightsail diameter compensated for by the restoring torques and forces inferred from experimentally characterized diffraction. Specifically, we observe that larger positive (negative) rotations require negative (positive) translations

https://doi.org/10.1021/acsphotonics.1c02022
ACS Photonics XXXX, XXX, XXX−XXX

for bounded motion, and similarly, larger positive (negative) translations can only be stabilized if the sail is initially rotated by a negative (positive) amount of rotation. This can be intuitively understood by looking at a specific case of initial conditions, for example, $x_0 = -0.1D$ and $\theta_0 = 3°$, where we plotted its trajectory during the first $50t_0$ with snapshots of the lightsail orientation shown at five different times (Figure 4h). For this example and in fact all four initial conditions $x_0 = \pm 0.1D$ and $\theta_0 = \pm 3°$, the trajectory of the propelled lightsail exhibits bounded dynamics, as illustrated by finite-amplitude oscillations of translation and rotation.

CONCLUSIONS

We have reported an optical design for passive stabilization of rigid lightsails and other macroscopic structures with extreme aspect ratios based on a monolithic and scalable material platform and fabricated a first suspended prototype of such metagratings in a silicon nitride membrane. By optically characterizing lightsails with judiciously chosen designs for anisotropic diffraction, using our custom-built angle-resolved photocurrent setup, we confirm the imparted passive stabilization mechanism by calculating self-stabilizing optically induced lateral force and in-plane torque from the measured refracted and reflected light intensities and angles. While achieving better agreement between experimental and simulated normalized intensities for each diffraction order would be desirable, we find that our lightsail prototype design already displays self-stabilizing behavior along one axis, as evidenced by numerical simulations of propulsion with experimental data as input functions. These results along with our error propagation analysis suggest that the intended careful balance between magnitudes and directions of all diffracted orders necessary for dynamical stability is achieved in our fabricated device, which differs from other design motifs in directing light into one particular order or maximizing the overall reflectance. With the focus of this report being on passive stabilization, which inherently reduces reflectance due to engineered scattering into higher diffraction orders, the propulsion force F_z being approximately half of the maximum achievable value at normal incidence offers room for improvement to minimize acceleration distance, as would be crucial for the Starshot mission. Future work should investigate the trade-off between dynamical stability and efficient propulsion and optimize for both, for example, by combining multiple photonic designs such as our metagratings with highly reflective photonic crystal arrays. We note that passive stabilization along two axes can be realized with composite metagrating designs by including a second orthogonally oriented metagrating design operating for transverse-magnetic polarization,[3] whose optical characterization can be readily performed in our setup by rotating both the sample and polarizer by 90°. A logical next step would be to directly quantify the mechanically self-restoring dynamics of our lightsail prototypes to radiation pressure by measuring actual displacement and rotation using optical characterization techniques such as interferometry and deflection spectroscopy during lightsail propulsion. Nonetheless, our results mark a first step toward characterizing nanophotonic structuring and shaping of diffraction of ultrathin silicon nitride membranes as a viable approach to realize future self-stabilizing laser-driven lightsails for spacecraft propulsion and contactless far-field optical manipulation.

METHODS

Perceptually uniform and undistorted color maps ("vik" and "batlowW") were used to represent the results in Figures 2b and 3d.[42,43]

Simulation and Fabrication. To study optical metagratings theoretically, we performed finite-element-method-based electromagnetic simulations in COMSOL Multiphysics. The dielectric function of silicon nitride at $\lambda = 514$ nm was determined using ellipsometry on unpatterned silicon nitride membranes, from which we fitted $n = 2.236$ and $k = 0.006$. Infinite periodic metagratings were modeled by applying Floquet periodic boundary conditions to a two-dimensional (2D) unit cell that comprises two rectangular suspended resonators. As we varied the period d accordingly together with the resonators' widths $w_{1,2}$ and their relative distance g, we systematically sampled the geometry space and calculated the induced optical pressures on the periodic structures using Maxwell's stress tensor. Assuming a beam with its electric field being parallel to the gratings (transverse-electric polarization) and a width of $w = 2D$ for finite-sized realizations of the metagratings, we calculated the lateral and vertical optical force and in-plane optical torque on a lightsail patterned mirror-symmetrically with the metagratings (see the Supporting Information). Self-stabilization, or marginal stability in the absence of natural damping mechanisms for lightsails in space, is characterized by the presence of purely imaginary eigenvalues in the Jacobian matrix derived from the lightsail's equations of motion in 2D. Consequently, we selected self-stabilizing metagrating designs based on the criteria of eigenvalues with zero real parts. We further narrowed down our portfolio of stable designs by comparing the slope and angular range of calculated lateral force and in-plane torque, resulting in the reporting self-stabilizing metagrating design ($d = 720$ nm, $h = 200$ nm, $w_1 = 170$ nm, $w_2 = 100$ nm, and $g = 95$ nm) shown in Figure 2a.

We fabricated self-stabilizing metagratings based on the optical design described above using low-stress 200 nm-thick silicon nitride membrane windows based on low-pressure chemical vapor deposition (Norcada). To define our metagrating design, we used electron-beam lithography to pattern a spun-on positive high-contrast resist (280 nm-thick ZEP 520A diluted to D.R. = 1.5). An additional conductive polymer of the same thickness was spin-coated on top of the resist to prevent the sample from charging. After resist development, the pattern was transferred into the membrane via inductively coupled reactive ion etching based on a SF_6/C_4F_8 chemistry. The remaining resist was stripped in multiple baths of heated NMP-based remover PG, after which the sample was thoroughly cleaned and dried. A more detailed description of fabrication steps and parameters is given in the Supporting Information.

Optical Characterization Setup. To characterize and verify the designed diffracting behavior of the fabricated self-stabilizing metagratings, we set up an angle-resolved photocurrent measurement apparatus (Figure 3a,b). The sample was mounted vertically onto a rotation stage for collimated light at 514 nm with a laser power of ~0.7 μW to be focused onto a spot of ~84 μm beam diameter on the sample by a 2× objective (NA = 0.055), resulting in an approximate laser power density of 253 W/m^2. To ensure that $\theta = 0°$ corresponds to the case of a normally incident focused laser beam, we first adjusted the tilt of the sample rotation stage

https://doi.org/10.1021/acsphotonics.1c02022
ACS Photonics XXXX, XXX, XXX−XXX

such that the specularly reflected order is aligned to the incident beam on the objective. For more precise alignment, we then measured the optical response of a nonblazed symmetrically diffracting grating fabricated on the same chip. The stage tilt at which t_{-1} and t_{+1} (or r_{-1} and r_{+1}) are equal corresponds to $\theta = 0°$, allowing us to determine θ with a small uncertainty of ~0.1°. A coaligned second rotation stage above the sample moves a rectangular planar photodiode (5 × 17 mm active area) on a circular path around the sample, allowing us to resolve the intensity and angle ϕ of refracted and reflected light versus incidence angle θ. We chose the specific photodiode to ensure that a portion of the light scattered out of the plane of rotation, for example, due to the anchor bars, is still being captured. Eucentric alignment is crucial to ensure that the beam shifts minimally when tilting the sample for non-normal incident light and to correctly map the photodiode position on the circular path to the diffracted order angles. A Python script was used to control both rotation stages, both of which were mounted onto *xyz* translation stages, and to run automated measurements.

■ ASSOCIATED CONTENT

Supporting Information

The Supporting Information is available free of charge at https://pubs.acs.org/doi/10.1021/acsphotonics.1c02022.

Fabrication of silicon nitride metagratings, calculation of optical forces and torques from measured scattering, calculation of the Jacobian matrix from equations of motion, fitting r_0 for small incidence angles, beam characterization, and error propagation analysis (PDF)

■ AUTHOR INFORMATION

Corresponding Author

Harry A. Atwater − *Thomas J. Watson Laboratories of Applied Physics, California Institute of Technology, Pasadena, California 91125, United States;* orcid.org/0000-0001-9435-0201; Email: haa@caltech.edu

Authors

Ramon Gao − *Thomas J. Watson Laboratories of Applied Physics, California Institute of Technology, Pasadena, California 91125, United States;* orcid.org/0000-0003-3591-7209

Michael D. Kelzenberg − *Thomas J. Watson Laboratories of Applied Physics, California Institute of Technology, Pasadena, California 91125, United States;* orcid.org/0000-0002-6249-2827

Yonghwi Kim − *Thomas J. Watson Laboratories of Applied Physics, California Institute of Technology, Pasadena, California 91125, United States;* Present Address: NTT Research Inc., Physics and Informatics Laboratories, 940 Stewart Drive, Sunnyvale, CA 94085, USA

Ognjen Ilic − *Department of Mechanical Engineering, University of Minnesota, Minneapolis, Minnesota 55455, United States*

Complete contact information is available at: https://pubs.acs.org/10.1021/acsphotonics.1c02022

Author Contributions

R.G. performed the numerical simulations, fabricated the device, performed the measurements, and analyzed the data. M.D.K conceived and built the setup and assisted with measurements. Y.K. developed the fabrication process and provided helpful comments on the device fabrication. O.I. provided insightful inputs to the numerical simulations and data analysis. R.G. and H.A.A. wrote the manuscript. All authors reviewed the paper. H.A.A. supervised the project.

Funding

This work was supported by the Air Force Office of Scientific Research (grant FA2386-18-1-4095) and the Breakthrough Initiatives, a division of the Breakthrough Prize Foundation.

Notes

The authors declare no competing financial interest.

■ ACKNOWLEDGMENTS

We would like to thank Dr. Lior Michaeli and Dr. Claudio Hail for their helpful discussions. We gratefully acknowledge the critical support and infrastructure provided for this work by the Kavli Nanoscience Institute at Caltech.

■ REFERENCES

(1) Atwater, H. A.; Davoyan, A. R.; Ilic, O.; Jariwala, D.; Sherrott, M. C.; Went, C. M.; Whitney, W. S.; Wong, J. Materials Challenges for the Starshot Lightsail. *Nat. Mater.* **2018**, *17*, 861−867.

(2) Breakthrough Starshot Initiative https://breakthroughinitiatives.org/initiative/3 (accessed on Dec 30, 2021).

(3) Ilic, O.; Atwater, H. A. Self-Stabilizing Photonic Levitation and Propulsion of Nanostructured Macroscopic Objects. *Nat. Photonics* **2019**, *13*, 289−295.

(4) Srivastava, P. R.; Chu, Y.-J. L.; Swartzlander, G. A. Stable Diffractive Beam Rider. *Opt. Lett.* **2019**, *44*, 3082.

(5) Srivastava, P. R.; Swartzlander, G. A. Optomechanics of a Stable Diffractive Axicon Light Sail. *Eur. Phys. J. Plus* **2020**, *135*, 570.

(6) Myilswamy, K. V.; Krishnan, A.; Povinelli, M. L. Photonic Crystal Lightsail with Nonlinear Reflectivity for Increased Stability. *Opt. Express* **2020**, *28*, 8223.

(7) Siegel, J.; Wang, A. Y.; Menabde, S. G.; Kats, M. A.; Jang, M. S.; Brar, V. W. Self-Stabilizing Laser Sails Based on Optical Metasurfaces. *ACS Photonics* **2019**, *6*, 2032−2040.

(8) Salary, M. M.; Mosallaei, H. Photonic Metasurfaces as Relativistic Light Sails for Doppler-Broadened Stable Beam-Riding and Radiative Cooling. *Laser Photon. Rev.* **2020**, *14*, 1900311.

(9) Salary, M. M.; Mosallaei, H. Inverse Design of Diffractive Relativistic Meta-Sails via Multi-Objective Optimization. *Adv. Theory Simul.* **2021**, *4*, 2100047.

(10) Gieseler, N.; Rahimzadegan, A.; Rockstuhl, C. Self-Stabilizing Curved Metasurfaces as a Sail for Light-Propelled Spacecrafts. *Opt. Express* **2021**, *29*, 21562.

(11) Kumar, A.; Kindem, D.; Ilic, O. Optomechanical Self-Stability of Freestanding Photonic Metasurfaces. *Phys. Rev. Appl.* **2021**, *16*, 014053.

(12) Taghavi, M.; Salary, M. M.; Mosallaei, H. Multifunctional Metasails for Self-Stabilized Beam-Riding and Optical Communication. *Nanoscale Adv.* **2022**, *4*, 1727.

(13) Rafat, M. Z.; Dullin, H. R.; Kuhlmey, B. T.; Tuniz, A.; Luo, H.; Roy, D.; Skinner, S.; Alexander, T. J.; Wheatland, M. S.; de Sterke, C. M. Self-Stabilization of Light Sails by Damped Internal Degrees of Freedom. *Phys. Rev. Appl.* **2022**, *17*, 024016.

(14) Chu, Y.-J. L.; Tabiryan, N. V.; Swartzlander, G. A. Experimental Verification of a Bigrating Beam Rider. *Phys. Rev. Lett.* **2019**, *123*, 244302.

(15) Chu, Y.-J. L.; Meem, M.; Srivastava, P. R.; Menon, R.; Swartzlander, G. A. Parametric Control of a Diffractive Axicon Beam Rider. *Opt. Lett.* **2021**, *46*, 5141.

(16) Ilic, O.; Went, C. M.; Atwater, H. A. Nanophotonic Heterostructures for Efficient Propulsion and Radiative Cooling of Relativistic Light Sails. *Nano Lett.* **2018**, *18*, 5583−5589.

(17) Ilic, O. Nanophotonic Materials for Space Applications. *MRS Bull.* **2020**, *45*, 769−778.
(18) Brewer, J.; Campbell, M. F.; Kumar, P.; Kulkarni, S.; Jariwala, D.; Bargatin, I.; Raman, A. P. Multiscale Photonic Emissivity Engineering for Relativistic Lightsail Thermal Regulation. *Nano Lett.* **2022**, *22*, 594−601.
(19) Tung, H.-T.; Davoyan, A. R. Low-Power Laser Sailing for Fast-Transit Space Flight. *Nano Lett.* **2022**, *22*, 1108−1114.
(20) Wilson, D. J.; Regal, C. A.; Papp, S. B.; Kimble, H. J. Cavity Optomechanics with Stoichiometric SiN Films. *Phys. Rev. Lett.* **2009**, *103*, 207204.
(21) Ftouni, H.; Blanc, C.; Tainoff, D.; Fefferman, A. D.; Defoort, M.; Lulla, K. J.; Richard, J.; Collin, E.; Bourgeois, O. Thermal Conductivity of Silicon Nitride Membranes Is Not Sensitive to Stress. *Phys. Rev. B: Condens. Matter Mater. Phys.* **2015**, *92*, 125439.
(22) Moura, J. P.; Norte, R. A.; Guo, J.; Schäfermeier, C.; Gröblacher, S. Centimeter-Scale Suspended Photonic Crystal Mirrors. *Opt. Express* **2018**, *26*, 1895−1909.
(23) Holdman, G. R.; Jaffe, G. R.; Jang, M. S.; Feng, D.; Kats, M. A.; Brar, V. W. Thermal Runaway of Silicon-Based Laser Sails. **2021**, arXiv Physics, arXiv:2110.06185 [physics.optics] (accessed 2022 -04-19).
(24) Zwickl, B. M.; Shanks, W. E.; Jayich, A. M.; Yang, C.; Bleszynski Jayich, A. C.; Thompson, J. D.; Harris, J. G. E. High Quality Mechanical and Optical Properties of Commercial Silicon Nitride Membranes. *Appl. Phys. Lett.* **2008**, *92*, 103125.
(25) Norte, R. A.; Moura, J. P.; Gröblacher, S. Mechanical Resonators for Quantum Optomechanics Experiments at Room Temperature. *Phys. Rev. Lett.* **2016**, *116*, 147202.
(26) Reinhardt, C.; Müller, T.; Bourassa, A.; Sankey, J. C. Ultralow-Noise SiN Trampoline Resonators for Sensing and Optomechanics. *Phys. Rev. X* **2016**, *6*, 021001.
(27) Tsaturyan, Y.; Barg, A.; Polzik, E. S.; Schliesser, A. Ultracoherent Nanomechanical Resonators via Soft Clamping and Dissipation Dilution. *Nat. Nanotechnol.* **2017**, *12*, 776−783.
(28) Gärtner, C.; Moura, J. P.; Haaxman, W.; Norte, R. A.; Gröblacher, S. Integrated Optomechanical Arrays of Two High Reflectivity SiN Membranes. *Nano Lett.* **2018**, *18*, 7171−7175.
(29) Wang, Y.; Stellinga, D.; Klemm, A. B.; Reardon, C. P.; Krauss, T. F. Tunable Optical Filters Based on Silicon Nitride High Contrast Gratings. *IEEE J. Sel. Top. Quantum Electron.* **2015**, *21*, 108−113.
(30) Nair, B.; Naesby, A.; Jeppesen, B. R.; Dantan, A. Suspended Silicon Nitride Thin Films with Enhanced and Electrically Tunable Reflectivity. *Phys. Scr.* **2019**, *94*, 125013.
(31) Parthenopoulos, A.; Darki, A. A.; Jeppesen, B. R.; Dantan, A. Optical Spatial Differentiation with Suspended Subwavelength Gratings. *Opt. Express* **2021**, *29*, 6481.
(32) Jin, W.; Li, W.; Orenstein, M.; Fan, S. Inverse Design of Lightweight Broadband Reflector for Relativistic Lightsail Propulsion. *ACS Photonics* **2020**, *7*, 2350−2355.
(33) Cheever, D. R.; Cad, F. M.; Klicker, K. A.; Stover, J. C. Design Review Of A Unique Complete Angle Scatter Instrument (CASI). *Current Developments in Optical Engineering II*; International Society for Optics and Photonics: San Diego, CA, United States, 1987; p 13.
(34) Amra, C.; Torricini, D.; Roche, P. Multiwavelength (0.45−10.6 μm) Angle-Resolved Scatterometer or How to Extend the Optical Window. *Appl. Opt.* **1993**, *32*, 5462−5474.
(35) Yang, N.; Angerer, W. E.; Yodh, A. G. Angle-Resolved Second-Harmonic Light Scattering from Colloidal Particles. *Phys. Rev. Lett.* **2001**, *87*, 103902.
(36) Neder, V.; Ra'di, Y.; Alù, A.; Polman, A. Combined Metagratings for Efficient Broad-Angle Scattering Metasurface. *ACS Photonics* **2019**, *6*, 1010−1017.
(37) Forward, R. L. Roundtrip Interstellar Travel Using Laser-Pushed Lightsails. *J. Spacecr. Rockets* **1984**, *21*, 187−195.
(38) Lubin, P. A. Roadmap to Interstellar Flight. *J. Br. Interplanet. Soc* **2016**, *69*, 40−72.
(39) Kulkarni, N.; Lubin, P.; Zhang, Q. Relativistic Spacecraft Propelled by Directed Energy. *Astron. J.* **2018**, *155*, 155.
(40) Parkin, K. L. G. The Breakthrough Starshot System Model. *Acta Astronaut.* **2018**, *152*, 370−384.
(41) Toft-Vandborg, C.; Parthenopoulos, A.; Darki, A. A.; Dantan, A. Collimation and Finite-Size Effects in Suspended Resonant Guided-Mode Gratings. *J. Opt. Soc. Am. A* **2021**, *38*, 1714.
(42) Scientific colour mapslZenodo https://zenodo.org/record/5501399 (accessed on Dec 30, 2021).
(43) Crameri, F.; Shephard, G. E.; Heron, P. J. The Misuse of Colour in Science Communication. *Nat. Commun.* **2020**, *11*, 5444.

https://doi.org/10.1021/acsphotonics.1c02022
ACS Photonics XXXX, XXX, XXX−XXX